Noncontact modulation calorimetry of metallic liquids in low Earth orbit

R. K. Wunderlich
Technical University Berlin, Metalphysics and Technology, Hardenbergstrasse 36, PN 2-3 10623 Berlin, Germany

D. S. Lee* and W. L. Johnson
California Institute of Technology, Keck Laboratory of Engineering Materials 138-78, Pasadena, California 91125

H.-J. Fecht
Technical University Berlin, Metalphysics and Technology, Hardenbergstrasse 36, PN 2-3 10623 Berlin, Germany
(Received 29 July 1996)

Noncontact modulation calorimetry using electromagnetic heating and radiative heat loss under ultrahigh-vacuum conditions has been applied to levitated solid, liquid, and metastable liquid samples. This experiment requires a reduced gravity environment over an extended period of time and allows the measurement of several thermophysical properties, such as the enthalpy of fusion and crystallization, specific heat, total hemispherical emissivity, and effective thermal conductivity with high precision as a function of temperature. From the results on eutectic glass forming Zr-based alloys thermodynamic functions are obtained which describe the glass-forming ability of these alloys. [S0163-1829(97)02302-3]

Precision measurements of the specific heat of stable and undercooled melts are of fundamental interest regarding the ultimate thermodynamic stability of undercooled melts and nonequilibrium crystals against vitrification and amorphization,[1] formation of associate structures in the melt,[2] the thermodynamic contribution to nucleation kinetics,[3] and thus the glass-forming ability of a material. In particular, Zr-based alloys have attracted considerable attention due to their glass-forming ability on rapid cooling,[4] solid-state amorphization reactions,[5] and, as base alloys of the recently discovered bulk glass formers.[6,7]

However, investigations of the thermophysical properties of the chemically reactive liquid metallic specimen at elevated temperatures are usually hampered using conventional techniques due to exothermic reactions with the container walls. Therefore, a containerless method has been developed which allows one to alleviate these problems.[8,9]

Due to insufficient temperature and positioning control of the samples of interest in an earth laboratory under UHV conditions the experiments have been performed in the space shuttle Columbia during the recent International Microgravity Laboratory 2 (IML-2) mission using the containerless electromagnetic processing (TEMPUS) device.[10] The absence of excessive heating and fluid flow associated with levitation under 1 g conditions assures quiescent sample conditions in an ultraclean environment ($<10^{-8}$ Torr base pressure) and precise modeling of the thermal balance.

Here, a metallic 8 mm diameter specimen (as an example $Zr_{64}Ni_{36}$) is heated by a 400 kHz radio frequency dipole field and positioned in the center of the heating coil by a 200 kHz quadrupole field. Temperature is measured by a high precision, <0.1 K, well calibrated two-color InAs pyrometer.

The different frequency and geometry of the heating and positioning fields allows separation of the total power input into additive components from heater and positioner, $P_{\mathrm{tot}} = P_H + P_{\mathrm{P_{Pos}}}$. The specimen equilibrium temperature T_0, is given by $P_{\mathrm{tot}} = A\sigma\varepsilon T_0^4$ with ε total hemispherical emissivity, A surface area and σ Stefan-Bolzmann constant. Induction heating of the levitated specimen can be discussed by analytical[11,12] and numerical methods including the induced force and fluid-flow fields.[13] The rate of Joule heat generated by the heater field is given as

$$P_H = 3\pi R(T)\rho(T)F(x)L\ I_H^2 = G_H(T)I_H^2 \tag{1}$$

with $R(T)$, $\rho(T)$, and I_H corresponding to radius, resistivity, and heater oscillating circuit current, respectively. The geometry factor L describes the relative position of heating coils and specimen. $F(x)$ accounts for the skin effect in a spherical sample with $x = R(T)/\delta(T)$ and δ skin depth. $F(x)$ is given in terms of analytical functions.[11,14] $G_H(T)$ defines the temperature-dependent heater coupling coefficient.

For heat-capacity measurements a sinusoidal modulation of heater current is applied, $I_H = I_{H0} + I_m \sin(\omega t)$, resulting in a heater power input:

$$P_H(t) = G_H(T)[I_{H0}^2 + \tfrac{1}{2} I_m^2 + 2I_{H0}I_m \sin(\omega_m t) + \tfrac{1}{2} I_m^2 \sin(2\omega_m t)] \tag{2}$$

and a steady state temperature response of the specimen given by

$$T(t) = T_0 + \Delta T_{\mathrm{av}} + \Delta T_m(\omega)\sin(\omega t + \phi_1) + \Delta T_{\mathrm{av}}(2\omega)\sin(2\omega t + \phi_2). \tag{3}$$

For each modulation frequency the heat capacity C_P of the specimen is connected with the amplitude of temperature modulation by[15]

$$C_P = f(\omega, \tau_1, \tau_2)\frac{P_m(\omega)}{\Delta T_m(\omega)\omega}. \tag{4}$$

$P_m(\omega)$ amplitude of power modulation at frequency ω $f(\omega, \tau_1, \tau_2)$ represents a correction function accounting for the effects of radiative heat loss with external relaxation

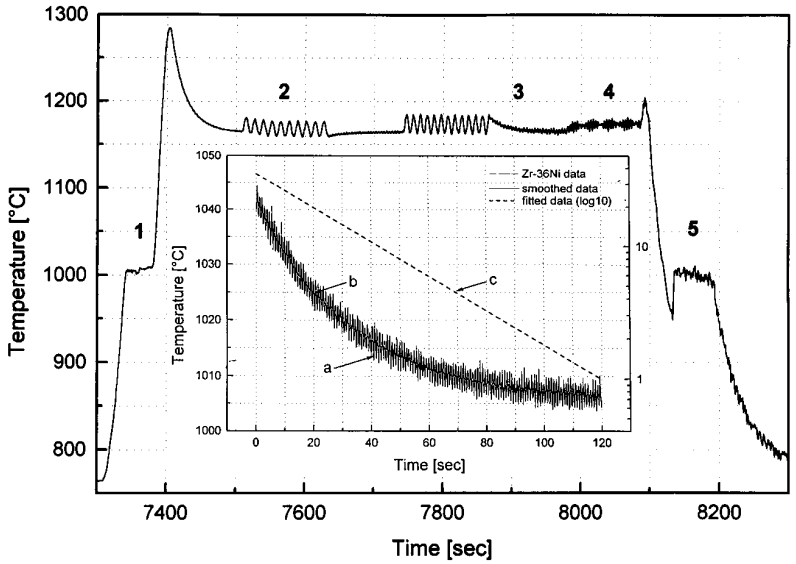

FIG. 1. Temperature-time profile of $Zr_{64}Ni_{36}$ specimen as processed in microgravity experiment. Inset shows temperature decay to equilibrium (a), FFT-filtered signal (b) and logarithmic plot (c) for τ_1 evaluation.

time τ_1 and finite thermal conductivity with internal relaxation time τ_2. For $\Delta T_{\rm av}/T_0 \ll 1$ the increase in the average temperature is given by

$$\Delta T_{\rm av} = \Delta P_{\rm av} \frac{\tau_1}{C_P}. \tag{5}$$

τ_1 is determined from measurements of temperature relaxation to equilibrium following a change in input power as

$$\tau_1 = (C_P/4\, A\ \sigma\ \varepsilon\ T_0^3), \tag{6}$$

allowing direct determination of ε from τ_1 and C_P measurements. For spherical symmetry and thermal conductivity κ the internal relaxation time is given by[8]

$$\tau_2 = (3C_P/4\pi^3 \kappa R). \tag{7}$$

Due to the widely different time scales of radiative heat loss and internal thermal conductance the low-frequency response of $\Delta T_m(\omega)$ is dominated by τ_1, while the high-frequency response is determined by τ_2. Adiabatic conditions are characterized by $\omega\tau_1/10 > 1 > 10\omega\tau_2$ and $f(\omega, \tau_1, \tau_2) \approx 1$, equivalent to $\Delta T_m(\omega)\omega = \text{const}$. As such, measurements of the frequency dependence of $\Delta T_m(\omega)$ allow identification of the adiabatic regime.

Figure 1 shows a typical experimental sequence performed in the space experiment on a $Zr_{64}Ni_{36}$ specimen. The enthalpy of fusion is determined from the duration of the isothermal melting (1) and recalescence plateau (5) at low undercooling. The specific heat is obtained from modulation experiments and from the increase in the average temperature upon application of heating power modulation (2). The total hemispherical emissivity is obtained from τ_1 measurements (3). Variation of the modulation frequency allows determination of an internal relaxation time (4), and an average value of the specific heat in the undercooled melt is obtained from measurements of the duration of the isothermal recalescence plateau as a function of undercooling (5). The inset shows the evaluation of the external relaxation time from temperature decay to equilibrium.

Quantitative evaluation of specific-heat values requires knowledge of the power component $P(\omega)$ and of the correction function $f(\omega, \tau_1, \tau_2)$. From Eq. (2), $P(\omega)$ and $\Delta P_{\rm av}$ are given in terms of heater current as

$$P(\omega) = 2G_H(T) I_{H0} I_m, \quad P_{\rm av} = \tfrac{1}{2}\, G_H(T) I_m^2. \tag{8}$$

In situ calibration experiments performed at $T_c = T_m - 40$ K where the specific heat is known independently from high-temperature differential scanning calorimetry (DSC) measurements provide $G_H(T_c)$. The modulation frequency was chosen such as to guarantee adiabatic conditions. The corresponding reference experiments were performed on identical solid 8 mm diameter spheres in a ground based experiment shown in Fig. 2 indicating an adiabatic regime for modulation frequencies in the range 0.05–0.2 Hz with an internal relaxation time $\tau_2 = 0.18$ s. From Eq. (7) a thermal conductivity of 0.25 W/cm K was obtained for the solid state in very good agreement with the Wiedemann-Franz law and a measured resistivity of 128 $\mu\Omega$ cm at T_c.

Describing the temperature dependence of $G_H(T)$ requires knowledge of the temperature dependence of resistivity and specimen radius including the change at T_m. The resistivity was determined *in situ* from measurements of the temperature dependence of the oscillating circuit current and

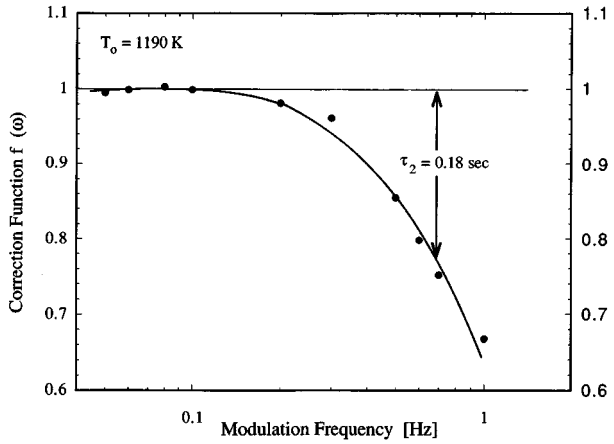

FIG. 2. Correction function $f(\omega, \tau_1, \tau_2)$ as function of modulation frequency.

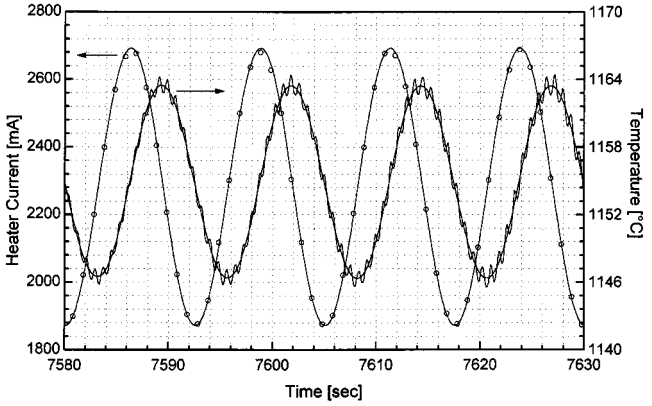

FIG. 3. Modulation experiment with liquid ZrNi specimen for $\omega_m = 0.08$ Hz. Heater current shown on left ordinate. Temperature response shown on right ordinate.

calibration with a specimen of known resistivity.[16] An upper limit of 3% for the volume change on melting could be inferred from analysis of video images of the specimen during processing in the TEMPUS facility in accordance with recently measured values for a similar glass forming alloy.[17] With these data the coupling function $G_H(T)$ has been obtained. By far, the main contribution to the temperature dependence of $G_H(T)$ arises from the resistivity change at T_m. As such $G_H(T)$ is rather insensitive to precise knowledge of the absolute temperature within ± 10 K. The advantage of modulation calorimetry calibration as compared to pulse heating experiments is that no knowledge of the emissivity is required and that it can be performed independently of the presence of a second heating field.

Figure 3 shows a recording of a modulation experiment at $\omega = 0.08$ Hz for a liquid specimen at $T_0 = 1420$ K. The driving heater current is shown on the left-hand ordinate. Open circles represent measured values sampled at 1 Hz allowing precise, $\pm 0.7°$, determination of the relative phase between heater current and temperature response. The additional high-frequency modulation in the temperature signal arises from sample movement in the potential well of the positioning field with eigenfrequencies near 1.2 Hz. The smooth curve represents a $\omega_L = 0.8$ Hz low pass fast-Fourier transform (FFT) filter. Fourier analysis of the temperature response reveals the presence of the 2ω modulation component according to Eq. (3). The amplitude of temperature modulation at frequency ω was obtained from the FFT-filtered curve after (i) correction for the transfer function of the low pass filter and (ii) subtracting the contribution of the 2ω component with proper phase resulting in a relative accuracy of 0.2 K for ΔT_m determination.

Adiabatic conditions in the liquid modulation experiments were verified by measurements of the phase shift between heater current and temperature. At $T_0 = 1430$ K values of $\phi_1 = -2.5$ mod $\pi/4$ and -3.4 mod $\pi/4$ were obtained for $\omega_m = 0.08$ and 0.10 Hz, respectively. With a measured external relaxation time of (22.1 ± 1) s this phase shift allows evaluation of the internal relaxation time as (0.24 ± 0.03) s indicating $1 - f(\omega, \tau_1, \tau_2) \leqslant 1 \times 10^{-2}$. From Eq. (7) a corresponding effective thermal conductivity of 0.25 W/K cm is obtained. For comparison, application of the Wiedemann-Franz law with a measured resistivity of 155 $\mu\Omega$ cm (Ref. 16) results in a thermal conductivity of 0.19 W/cm s and $\tau_2 = 0.32$ s. This apparent increase in the measured effective thermal conductivity is due to the effect of electromagnetic stirring of the liquid and may serve to distinguish different fluid-flow models.

TABLE I. Specific heat of $Zr_{64}Ni_{36}$. (mod): results obtained by modulation calorimetry; (av): results obtained from ΔT_{av} and τ_1 measurements.

T_0(°C)	ω_m (Hz)	c_p (mod) (J mol^{-1} K^{-1})	c_p (av) (J mol^{-1} K^{-1})	τ_1 (s)	ε_{tot}
1215	0.05	43.7±0.8	43.0±2	18.2±1	0.38
1160	0.08	44.5±1.2	43.0±4	21.8±1	0.36
	0.10	43.2±1	43.5±2		
1038	0.05	43.9±1	41.2±2	30.0±0.6	0.34
	0.08	44.2±1	43.9±2		
1008	0.05	44.0±1	44.7±2	33.0±1	0.33
	0.10	44.6±1	45.7±2		
980	0.05	45.5±1.2		36.9±2	0.32
960	0.08	32.0±1	32.0±1	30.8±1	0.30
solid, T_c					

Table I exhibits specific heat values obtained by modulation calorimetry and those obtained from measurements of ΔT_{av} and τ_1. The good agreement between c_p values at different modulation frequencies indicates the absence of effects caused by transient internal temperature gradients. Values of the total hemispherical emissivity ε_H are shown in the last column with the liquid values exhibiting a $\sqrt{\rho T}$ temperature dependence.

Determination of the thermodynamic functions requires knowledge of the enthalpy of fusion which can be obtained from the power balance pertaining to the isothermal melting or solidification plateau. Input power is given by the rate of crystallization enthalpy release and by the combined action of heating and positioning fields while output is determined by purely radiative heat loss. Figure 4 shows temperature and heater current of a recalescence event at low undercooling, $\Delta T_u \approx 10$ K, used for the evaluation of the enthalpy of crystallization. The heating efficiency of the positioner field, $G_{\text{Pos}}(T)$, can be evaluated from modulation measurements at T_c with temperature scaling similar to $G_H(T)$.[18] The change in heater current shown in Fig. 4 results from the resistivity change at T_m and was used to scale $G_H(T_m, t)$ and $G_{\text{Pos}}(T_m, t)$ as a function of time between liquid and solid values. As solidification proceeds rapidly on the surface of the droplet the emissivity during solidification was taken to correspond to that of the solid at T_c. We thus obtain $\Delta H_f = (14.4 \pm 0.4)$ kJ mol^{-1} including a contribution of 0.45 kJ mol^{-1} from heating the undercooled melt by $\Delta T_u \approx 10$ K. Knowledge of ΔH_f allows determination of the average specific heat in the temperature interval ΔT_u from measurements of the duration of the isothermal recalescence plateau as a function of undercooling.[19] The resulting specific-heat values of $Zr_{64}Ni_{36}$ obtained in this experiment are summarized in Fig. 5. The lower curve represents crystalline values obtained by conventional DSC measurements, while the upper curve represents data in the stable and undercooled melt with a maximum undercooling of 80 K. Squares represent

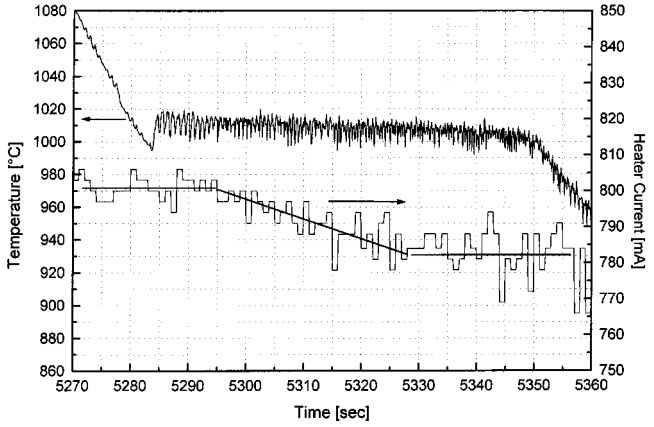

FIG. 4. Recalescence event. Left ordinate: temperature; right ordinate: rf-heater generator current.

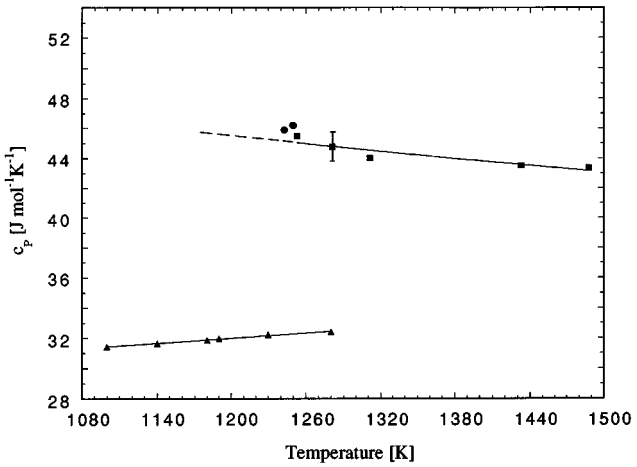

FIG. 5. Specific heat of $Zr_{64}Ni_{36}$. Lower curve crystalline solid. Upper curve liquid; full squares: values obtained by modulation calorimetry, full circles: values of the average specific heat in the undercooled regime.

data obtained by modulation calorimetry, while the full circles represent the average specific heat in the undercooled melt showing an increase of the liquid specific heat with decreasing temperature typical for glass-forming alloys.

Liquid specific-heat data were linearly extrapolated for an estimate of the thermodynamic functions in the undercooled melt according to

$$c_P^1(T) = (55.02 - 8.0 \times 10^{-3}\ \mathrm{T})\ \mathrm{J\,mol^{-1}\,K^{-1}}. \qquad (9)$$

From the Kauzmann stability criterion, $\Delta S^{1,x}(T_{g0}) = 0$, the reduced glass transition temperature $T_{g0} = T_m / T_g$ was obtained as $T_{g0} = 0.51$ which places the ZrNi binary eutectic at an intermediate position between the bulk glass formers with $T_{g0} = (0.64 \pm 0.3)$ and a typical extrapolated value of $T_{g0} = 0.32$ for pure metals.[20] The value of T_{g0} thus obtained is in good agreement with recent model calculations[21] for this system, $T_{g0} = 0.49$, and an upper limit of $T_{g0} = 0.50$ obtained from crystallization of rapidly quenched splats.[22] Furthermore, the driving force for crystallization, $\Delta G^{1,x}(T)/\Delta H_f$, of the binary ZrNi eutectic in comparison with a pure metal[20] at a critical undercooling $T_u = 0.5\ (1 + T_{g0})$ corresponds to 0.22 and 0.32, respectively, equivalent to at least five orders of magnitude difference in critical cooling rates for glass formation.

We acknowledge stimulating discussions with Professor G. Frohberg (TU-Berlin), Professor William Hofmeister (Vanderbilt University), and Dr. G. Lohöfer (DLR Cologne) and the excellent support of the MUSC team at DLR Cologne. R.K.W. and H.J.F. acknowledge financial support from DARA (Grant No. 50 WM 94-31-4), D.S.L. and W.L.J. from NASA (Grant No. NAG8-954/NAG9-1192).

*Present address: Amorphous Technologies International, 27722 El Lazo, Laguna Niguel, CA 92656.

[1] H. J. Fecht and W. L. Johnson, Nature (London) **334**, 50 (1988).
[2] F. Sommer, Z. Metallkd. **73**, 77 (1982).
[3] D. Turnbull, J. Chem. Phys. **20**, 411 (1952); F. Spaepen, Acta Metall. **23**, 729 (1975).
[4] K. H. J. Buschow, B. H. Verbeek, and A. G. Dirks, J. Phys. D **14**, 1087 (1981).
[5] W. L. Johnson, Prog. Mater. Sci. **30**, 81 (1986).
[6] A. Peker and W. L. Johnson, Appl. Phys. Lett. **63**, 2342 (1993).
[7] A. Inoue, T. Zhang, N. Nishiyama, K. Ohba, and T. Masumoto, Mater. Trans. JIM **35**, 1234 (1993).
[8] H.-J. Fecht and W. L. Johnson, Rev. Sci. Instrum. **62**, 1299 (1991).
[9] R. K. Wunderlich, R. Willnecker, and H.-J. Fecht, Appl. Phys. Lett. **62**, 3111 (1993).
[10] Team TEMPUS, in *Materials and Fluids Under Low Gravity*, edited by L. Ratke, H. Walter, and B. Feuerbacher, Springer Lecture Notes in Physics (Springer, Berlin, 1995).
[11] E. Fromm and H. Jehn, Z. Metallkd. **58**, 366 (1967).
[12] G. Lohöfer, Int. J. Eng. Sci. **32**, 107 (1994).
[13] J. H. Zhong, B. Li, and J. Szekely, Acta Astron. **29**, 305 (1993).
[14] B. Q. Li, Int. J. Eng. Sci. **31**, 201 (1993).
[15] Y. A. Krafmakher, High Temp. High Pressures **24**, 145 (1992).
[16] G. Lohöfer (unpublished).
[17] H.-J. Fecht, S. G. Klose, and M. P. Macht, in *Proceedings of the 2nd Pacific Rim International Conference on Advanced Materials and Processing*, edited by K. S. Shin, J. K. Yoon, and S. J. Kim (The Korean Institute of Metals and Materials, Seoul, 1995), p. 2155.
[18] R. K. Wunderlich and H.-J. Fecht, Int. J. Thermophys. (to be published).
[19] A. J. Rulison and W. K. Rhim, Rev. Sci. Instrum. **65**, 695 (1994).
[20] H.-J. Fecht, Mater. Trans. JIM **36**, 777 (1995).
[21] T. Aihara, Jr., K. Aoki, and T. Masumoto, Mater. Trans. JIM **36**, 399 (1995).
[22] Z. Altounian, Tu Guo-hua, and J. O. Strom-Olsen, J. Appl. Phys. **54**, 3111 (1983).